Grain Shapes and Growth Kinetics of the Cylinder Phase in a Block Copolymer Solution

Thomas Q. Chastek and Timothy P. Lodge*,†

Department of Chemistry, University of Minnesota, Minneapolis, Minnesota 55455-0431

Received March 12, 2004; Revised Manuscript Received April 19, 2004

ABSTRACT: The ordering kinetics of the cylinder phase were characterized using polarizing optical microscopy (POM). Measurements were made on a poly(styrene-*b*-isoprene) diblock copolymer with block lengths of 15 and 13 kg/mol, respectively, in solution with dibutyl phthalate at a polymer volume fraction of 0.50. Thermal quenches from above the disordering temperature, 39.6 °C, to temperatures ranging from 36.5 to 38.4 °C allowed for direct observation of nucleation and growth. Two modes of grain growth were observed after nucleation: spherulites and oblate ellipsoids. The ellipsoidal grains had an aspect ratio of 2 and corresponded to single crystals with the cylinders parallel to the minor axis of the ellipsoid. In contrast, the spherulites were polycrystalline, with the cylinder axes predominantly tangential to the spherulite. Ellipsoids and spherulites occurred with comparable frequency at all quench depths. The growth front velocities of individual grains were measured, and the velocities for spherulites and for the major axes of the ellipsoids were approximately twice that along the minor axis of the ellipsoids. The growth front velocities were quantitatively compared to the expression of Goveas and Milner, with good agreement in the temperature dependence. Application of the Avrami equation to the observed ordered fraction yielded parameters in good agreement with those inferred microscopically for heterogeneous nucleation and three-dimensional growth.

Introduction

An exciting avenue of block copolymer research is in understanding nonequilibrium phase behavior. The ordering kinetics of various block copolymer nanostructures have been characterized by observing the evolution of a given experimental parameter over time, following a thermal quench through the order−disorder transition temperature (T_{ODT}). Insight into the dominant nucleation modes, grain growth front velocities, and grain shapes has been gained. A variety of techniques have been used to make kinetic measurements, including small-angle X-ray and neutron scattering (SAXS, SANS),[1−17] rheology,[4−8,18,19] depolarized light scattering,[20−27] transmission electron microscopy (TEM),[1−3,28] polarized optical microscopy,[29] and birefringence.[9]

In this paper we focus on the kinetics of ordering of the cylinder phase in a block copolymer solution. Bulk kinetics of cylinder formation has previously been probed with SAXS and rheology.[2,4,5,8] For example, Floudas et al.[8] characterized the fraction of cylinder formation over time, $\phi_c(t)$, by tracking changes in the dynamic moduli after a temperature quench from above T_{ODT}. In addition, they used SAXS to determine $\phi_c(t)$ by recording the change in scattering power after thermal quenches. On the basis of the Avrami exponent values of 3 for shallow quenches, they concluded that ordering proceeded by heterogeneous nucleation followed by three-dimensional growth.

Growth front velocities of individual grains during cylinder formation have been measured by Balsara et al.[24] They used depolarized light scattering to infer details of grain size, shape, and concentration as a function of time following thermal quenches through T_{ODT}. The experimentally determined grain growth front velocities were compared to the relationship of Goveas and Milner,[30] which predicts growth front velocities based on experimentally measurable parameters such as the chain relaxation time, end-to-end distance, and the Flory−Huggins interaction parameter. Balsara et al. were subsequently able to demonstrate that the Goveas and Milner relationship correctly predicted the temperature dependence of the grain growth front velocity.[21]

Characterization of cylinder grain shapes induced by thermal quenches has been made directly using TEM[2,31] and indirectly using depolarized light scattering.[26] Sakamoto et al. examined a poly(styrene-*b*-isoprene-*b*-styrene) triblock in solution with dioctyl phthalate and found cylinder grains to be "lenslike" oblate ellipsoids with the cylinders parallel to the minor ellipsoid axis and having aspect ratios of 3.5.[2] While TEM provided direct visualization of grains, it was limited in the volume of sample that could be observed, and any given grain could be observed in only one plane. The observations of Balsara and co-workers,[26] who used depolarized light scattering, are in apparent disagreement with those of Sakamoto et al. Specifically, the scattering profiles of Balsara and co-workers were best fit with a prolate ellipsoid shape with the cylinders parallel to the major ellipsoid axis. Subsequent depolarized light scattering measurements were consistent with these results;[21,24,32] the grains had aspect ratios of about 4 at early stages, which decreased over time. It should be noted, however, that Balsara and co-workers specifically ruled out the possibility that the grains were oblate ellipsoids only once,[32] and this experiment was different from the work of Sakamoto et al. because it examined a larger quench depth. The theoretical work of Wickham et al.[33] found "lenslike" grains with aspect ratios of 4−10, in better agreement with the shape proposed by Sakamoto et al.

† Also Department of Chemical Engineering and Materials Science.

* Author for correspondence: lodge@chem.umn.edu.

10.1021/ma049502d CCC: $27.50
Published on Web 05/29/2004

In this work we characterize the ordering of poly(styrene-*b*-isoprene) in dibutyl phthalate (DBP) into cylinders after a thermal quench below T_{ODT}. DBP is a selective solvent, which preferentially swells the polystyrene microdomains. The equilibrium phase behavior of this sample was previously reported.[34] POM was used for time-resolved real space analysis of the grain shape, grain growth front velocities, and the bulk kinetics. Grains were rotated about an axis perpendicular to the light beam, allowing detailed characterization of the three-dimensional shape. Growth front velocities of individual grains were directly visualized and were compared quantitatively to the Goveas−Milner prediction.[30] Also, direct observations of the nucleation and growth mechanism were compared to conclusions drawn from "macroscopic" analysis using the Avrami equation.

Experimental Section

Materials. The polymer investigated was poly(styrene-*b*-isoprene) with block molecular weights of 15 and 13 kg/mol, respectively, and denoted SI(15−13). The synthesis and characterization of SI(15−13) are described elsewhere.[34] Measurements were made on SI(15−13) dissolved in dibutyl phthalate (DBP) at 50 vol % of polymer. A homogeneous solution was prepared by codissolving SI(15−13) and DBP in methylene chloride and subsequently removing the methylene chloride with a gentle flow of nitrogen for 2−4 days. The DBP was purchased from Aldrich and purified by washing with 5% aqueous sodium bicarbonate followed by repeated washing with distilled water. It was dried over calcium chloride for 1−2 days to remove any residual water. The T_{ODT} was determined from polarizing optical microscopy to be 39.6 ± 0.2 °C. The transition was identified visually upon slow heating, which was possible because the birefringent ordered cylinder phase was clearly distinguishable from the isotropic disordered state. Measurements of T_{ODT} by other techniques confirm this result: SAXS, 40 ± 2 °C; rheology, 40 ± 1 °C; static birefringence, 40 ± 1 °C.

Polarized Optical Microscopy (POM). POM is a direct means of observing formation of the birefringent cylinder phase from an isotropic disordered state. The difference in birefringence made the disordered state and cylinder phase clearly distinguishable at the magnifications that were investigated. A partial waveplate was inserted between the polarizer and the sample to increase the contrast between the birefringent and nonbirefringent regions. The waveplate partially depolarized the light, making nonbirefringent regions appear a uniformly gray. Birefringent regions either increased (light colored) or decreased (dark colored) the effect of the waveplate, depending on the cylinder orientation.

Measurements were made using either a Nikon Optiphot-Pol or an Olympus BX51 optical microscope. A Linkam DSC with attached liquid nitrogen pump was used as a sample holder to control the temperature in quenching experiments. Samples were pressed between two 1 mm thick glass disks to a thickness of 100−150 μm and sealed with silicone glue. The Linkam DSC allowed for rapid temperature quenches (>20 °C/min cooling) with no overshoot and temperature stability to ±0.1 °C. This allowed for resolution of quench depths ca. 0.3 °C apart. Furthermore, the cooling rate was rapid enough to ensure that the cooling process did not affect the subsequent kinetic measurements. Temperature-jump measurements entailed annealing the sample at 45 °C for 5 min to form a fully disordered fluid. The temperature was then lowered rapidly in one step to the temperature of interest. The temperature went from T_{ODT} to a stabilized final temperature in 10−20 s depending on the quench depth. For comparison, the half-lives of the transitions ranged from 2 to 30 min. Measurements were made from 1.2 to 3.1 °C below T_{ODT}.

Additional measurements were made with a custom-made aluminum heating block connected to a Fenwal 921 temperature controller, allowing for temperature stability to ±0.2 °C. The heating block allowed for samples to be viewed while sealed in 1.5 mm glass capillaries (Charles Supper Co.). The capillaries were sealed with silicone glue. Refractive aberrations were reduced by viewing the capillaries between two flat slides in a refractive index matching oil (Cargille Co. type B oil). The capillaries were measured on their side and rotated about their central axis. That is, the rotation of the capillary changed the imaging plane. This allowed for detailed characterization of the three-dimensional shape of the grain.

Small-Angle X-ray Scattering (SAXS). SAXS measurements were made on the University of Minnesota 2-D 6m SAXS line, which uses Cu Kα X-rays (λ = 1.54 Å) from a Rigaku Ultrex 18 kW generator. The sample chamber and optics were filled with helium, while the flight tube was under vacuum. The sample-to-detector distance was 258 cm. The images were corrected for detector response. The samples were measured in the same capillaries as in POM. All measurements were made at room temperature.

Rheology. Rheological measurements were made with an ARES instrument (Rheometric Scientific), with 25 mm parallel plates at a gap of ca. 1 mm. Viscosity values were ascertained by measuring the frequency dependence of the dynamic moduli at fixed temperature and taking the low-frequency limiting value of (G''/ω).

Results and Discussion

Experimental observations mainly consisted of polarizing optical microscopy (POM) measurements of SI(15−13) in DBP. POM was found to be a straightforward means of making a comprehensive examination of cylinder ordering kinetics. Observations include detailed characterization of the three-dimensional cylinder grain shape, direct visualization of grain growth front velocities, and characterization of the bulk kinetics.

Grain Shapes. Detailed visual observation of SI(15−13) in DBP provided a thorough characterization of the emerging grain shapes. Surprisingly, there were two distinct modes of grain growth observed: oblate ellipsoids and spherulites. The former was anticipated and was broadly consistent with the "lenslike" shape observed by Hashimoto and co-workers[2,31] and predicted by Wickham et al.[33] The spherulitic grains, however, were not anticipated given the current understanding of the cylinder ordering process.

A typical ellipsoidal grain is depicted in Figure 1 through a sequence of micrographs of a single ca. 300 μm diameter cylinder grain at fixed resolution in a matrix of isotropic, disordered fluid. Throughout the sequence of images, the sample is progressively rotated about an axis along the horizontal plane of the micrographs. The grain of interest formed after a shallow thermal quench ($T_{ODT} - T$ = 1.2 ± 0.2 °C). The temperature was lowered slowly (approximately 1 °C/3 min) to avoid undercooling, and the sequence of images was taken over the course of 10 min, roughly 1 h after the temperature quench. The grain grew at ca. 5 μm/min, thereby increasing in size by 20% during this measurement. Note also that there were often ca. 10 μm particles on the surface of the capillary tubes as received. The particles are visible in some micrographs, with their size often exaggerated by being out of focus. The capillary tubes were repeatedly washed with methylene chloride to remove as many particles as possible. The specific grain shown in Figure 1 nucleated and grew in the center of the capillary where the concentration of these particles was low.

Figure 1a shows a view of the grain in an orientation where it is highly birefringent and has an aspect ratio of ca. 2. The lines spanning the grains are measure-

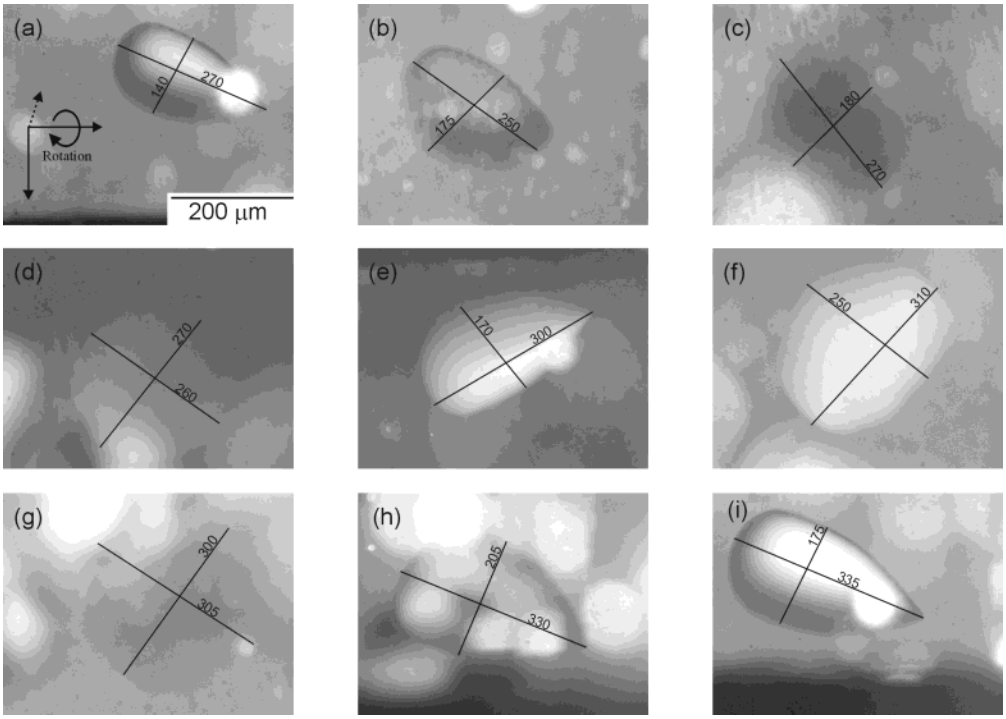

Figure 1. Rotation of an ellipsoid grain. A single birefringent cylinder grain is observed in an isotropic disordered matrix after a shallow quench ($T_{ODT} - T = 1.2 \pm 0.2$ °C). The grain is rotated about an axis as shown in (a). The approximate degrees of rotation are (a) 0°, (d) 90°, (e) 180°, (g) 270°, and (i) 360°.

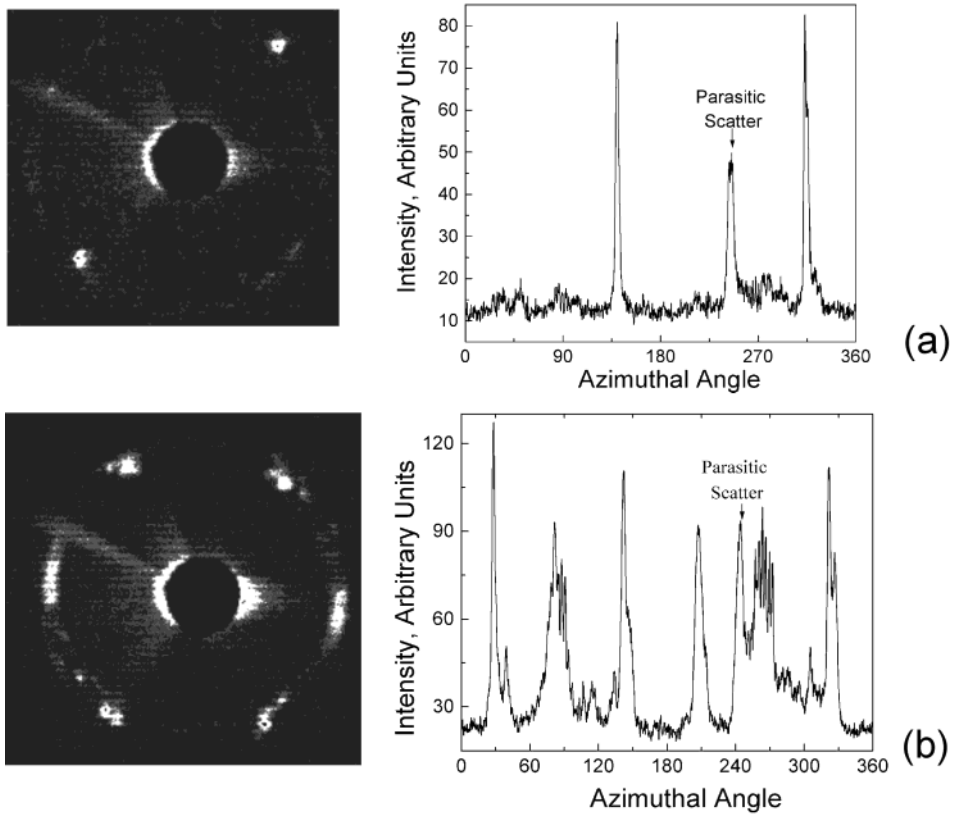

Figure 2. SAXS profiles of cylinder grains and the corresponding azimuthal integration. Measurements were made where the X-ray beam passes predominantly through large single domain grains with the beam aligned (a) perpendicular and (b) parallel to the cylinder axis.

ments of the shorter and longer axes in micrometers. As the grain is progressively rotated by 90° (Figure 1a–d), the shorter axis increases while the birefringence decreases. In Figure 1d the grain is nearly nonbirefringent, and both the length and width of the grain are equal to the long axis in Figure 1a. This indicates that the grain is an oblate ellipsoid. When the grain was in the orientation of Figure 1d, it could be rotated about the beam axis, and no change in birefringence was observed. Thus, it can be concluded that the cylinder

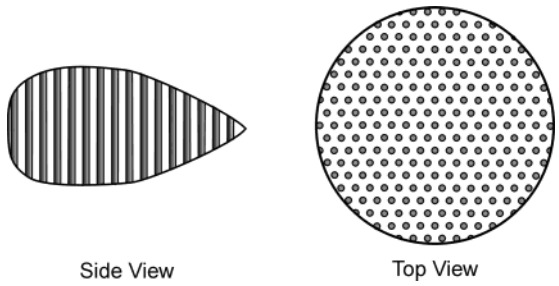

Figure 3. Schematic representation of observed ellipsoid grains. The side view shows the cylinders are aligned along the minor axis of the grain.

axis is parallel to the beam path in Figure 1d. That is, the cylinders are aligned parallel to the minor axis of the oblate ellipsoid, which is consistent with the findings of Hashimoto and co-workers.[2,31] Also, it should be noted that while Figure 1d is slightly birefringent, the grain does become completely nonbirefringent with a slightly smaller amount of rotation. Identification of grain dimensions, however, cannot be made at the nonbirefringent orientations.

The grain has been rotated approximately 180° by Figure 1e. Since a partial waveplate was used, the grain color changes from dark gray to white between parts a and e of Figure 1. The color change is caused by the change in cylinder orientation. The cylinder orientation in Figure 1a counteracts the effect of the waveplate, and the cylinder orientation in Figure 1e enhances it. The grain has been rotated by 270° in Figure 1g and is once again nonbirefringent. Finally, the 360° revolution is complete in Figure 1i. The grain grew slightly during the process of capturing images, but the aspect ratio remained at ca. 2.

To corroborate that the grains being observed with POM were single crystals, and not polycrystalline aggregates, SAXS measurements were made. The protocol consisted of slowly quenching the sample just below T_{ODT} and allowing a few large grains (up to 1 mm in diameter) to grow in the capillaries. The capillary was rotated and positioned in the X-ray beam to locate single grains. Figure 2 shows two typical SAXS patterns and their corresponding azimuthal integrations. The two-spot pattern in Figure 2a corresponds to hexagonally packed cylinders where the beam passes predominantly through a grain having cylinders aligned perpendicular to the X-ray beam. The six-spot pattern with 60° spacing shown in Figure 2b corresponds to the orientation where the beam passes predominantly through a grain having cylinders aligned parallel to the beam. The dominance of the two-spot and six-spot patterns indicates that the X-ray beam (approximately 1 mm in width) is incident mainly on large, single-crystal grains.

While the measurements of the ellipsoid grains are broadly consistent with the results Hashimoto and co-workers[2,31] and Wickham et al.,[33] there are some differences. For example, instead of a "lenslike" grain, a "clamlike" grain was observed where the cylinder length is not a uniform function of distance from the center point. Figure 3 is a schematic drawing that summarizes the observed ellipsoid grain shape. The side view shows that grain is tapered at only one end instead of both. The top view shows that the grains in this orientation were observed to be circular and have the cylinder axis pointing normal to this plane. In addition, the typical aspect ratio of the ellipsoid grains (ca. 2) was found to be smaller than the values observed by Koisumi et al. (3.5)[31] or predicted by Wickham et al. (4−10).[33] It is not clear why the "clamlike" grains are observed. Both the tapered and blunt ends grow at the same rate, suggesting that the blunt end does not result from impaired growth. Also, at greater quench depths, the tapered end is not observed, and ellipsoids are uniformly blunt. There may not be a strong thermodynamic preference for blunt or tapered edges, but the blunt end appears to be kinetically favored.

A possible explanation for the presence of ellipsoidal grains was put forth by Koisumi et al. based on anisotropic interfacial surface tension.[31] They contended that the ends of individual cylinders exposed to the disordered matrix have very highly curved "microinterfaces". This would potentially decrease the surface tension of the cylinder end "macrointerface" (i.e., the surface of the grain associated with the cylinder ends) by allowing for increased packing space for the polystyrene block at each cylinder end. The reduced surface tension at the cylinder ends slows cylinder lengthening, which leads to oblate ellipsoid grains.

Ellipsoid grains have also been observed in lamellae ordering.[1,28,35,36] Balsara et al. calculated a lamellar grain shape using the Wulff construction, and the agreement with experimental observations indicated that the ellipsoidal grain shape was due to anisotropic interfacial tension.[37] It is interesting that our observed aspect ratio of 2 in cylinder ordering is comparable to that observed experimentally and theoretically in lamellar ordering.[36,37] When cylinders are viewed end-on, and lamellae edge-on, the average surface composition matches the bulk composition, whereas when cylinders are viewed edge-on, and lamellae face-on, the instantaneous surface composition is usually different from the bulk, leading to higher surface energies and larger growth rates.

Unexpectedly, the cylinder ordering did not occur exclusively through single-crystal ellipsoid grains. There were significant numbers of spherulite grains present at all quench depths. An example of a spherulite is shown in Figure 4. The insets in the lower right corners show the grain after the removal of the partial waveplate. This makes evident the presence of the Maltese cross, the defining characteristic of spherulites. Furthermore, Figure 4b shows the same grain after a 90° rotation about the horizontal axis of the image plane (indicated in Figure 4b). The round shape remains, which demonstrates the spherical shape of the grain. Furthermore, knowing the cylinder orientation in the ellipsoid grains, the orientation of cylinders in the spherulites can be deduced. Figure 5a shows a representative micrograph of a temperature quench experiment in the early stages of ordering. Several birefringent grains are visible in the isotropic disordered matrix. Figure 5b is a schematic representation of three grains visible in the micrograph. Single headed arrows have been drawn as reference markers to distinguish the grains of interest. In particular, the outlines of grains 1 and 2 lack some clarity due to superposition with other grains. Grains 1 and 2 are ellipsoids with cylinders oriented parallel to the minor axis. The cylinder axes are indicated with double-headed arrows in Figure 5b. Grain 3 is a spherulite. The cylinder axis in grain 1 goes from upper-left to lower right in the image, and this orientation counteracts the effect of the waveplate (dark colored). Likewise, the cylinder axis in grain 2 lies from upper right to lower left in the image

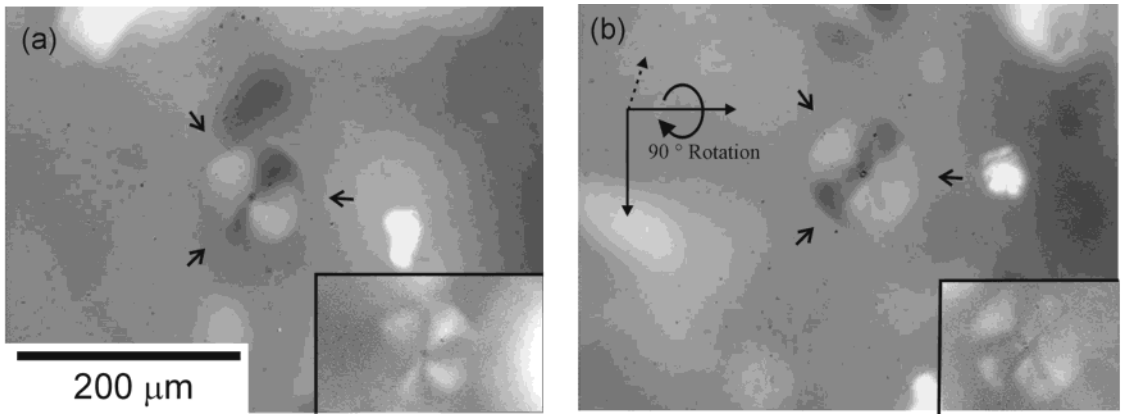

Figure 4. Images of a single spherulite grain at different orientations. In (b) the spherulite grain was rotated 90° about an axis shown in the image. The insets in the lower right corners show the spherulite after removal of the partial waveplate.

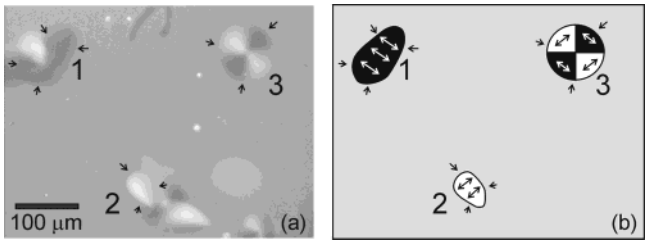

Figure 5. Cylinder orientation in spherulites. (a) A micrograph of cylinder formation in a disordered matrix 3 min after a quench to 37.8 °C. There are three grains of interest. Grains 1 and 2 are ellipsoids, and grain 3 is a spherulite. Single-headed arrows are reference markers to locate the grain. (b) A schematic representation of the micrograph. Double-headed arrows indicate the orientation of the cylinders.

and enhances the effect of the waveplate (light colored). There are two possible average arrangements of cylinders in a spherulite: tangential and radial. The tangential arrangement is consistent with the ellipsoid grain, while the radial arrangement is not. That is, the light regions of grain 3 have cylinders pointing upward from left to right, and the dark regions have cylinders pointing downward from left to right. Thus, grains of ordering cylinders were observed to be shaped either as "clamlike" oblate ellipsoids with cylinders lying along the minor axis or as spherulites with cylinders mainly arranged tangentially.

Nucleation. POM provides insight into the nucleation mode during cylinder ordering. It was observed that the ordering occurred through heterogeneous nucleation. In some cases heterogeneous nucleating agents were clearly visible; for example, the center of the spherulite shown in Figure 4 has a distinct nucleating particle. It was also observed that rapid nucleation occurred in the early stages of the transition, with little subsequent nucleation, which is consistent with a heterogeneous process. Finally, as shown in Figure 6, repeated quenches from disorder gave rise to nucleation at the same sites. Figure 6 shows measurements of three different quenches from disorder for a fixed field of view. Three grains are pointed out which were found to nucleate at identical positions. (Note that the nucleation densities are not uniform because the quench depth varied.)

These nucleation events give rise to either spherulites or ellipsoid grains, apparently randomly. Figure 7 shows the nucleation density of ellipsoids and spherulites at several quench temperatures. At all quench temperatures measured, there are roughly equal proportions of both types of grains. Furthermore, as seen in Figure 6, given nucleation sites can give rise to either type of grain. In Figure 6a two ellipsoidal grains and one spherulite form, whereas in Figure 6c the same nucleation sites give rise to three spherulites. In Figure 6c, the quench was deeper, but this does not mean that the deeper quenches necessarily favor spherulites. In fact, sites which on one occasion give rise to spherulites at shallow quenches have been observed on another occasion to give rise to ellipsoids at deeper quenches. Figure 6b exhibits a grain which initially was an ellipsoid but partially converted to a spherulite. This phenomenon will be discussed more in the following section.

Growth Front Velocities. POM allowed measurement of the growth front velocities of individual grains, as described in detail previously.[29] Growth front velocities were measured for several quench depths below T_{ODT}. For each quench experiment, selected grains with minimal impingement or superposition of other grains were measured over time. It was found that for all grain types and at all quench depths the growth fronts propagated at a constant, temperature-dependent velocity throughout the ordering process. Since there was a mixture of ellipsoids and spherulites, three categories of growth front velocities were measured: spherulite ($\nu_{spherulite}$), major axis of ellipsoid (ν_{major}), and minor axis of ellipsoid (ν_{minor}). These values are presented in Figure 8. The data points represent the average growth front velocities for multiple grains. The error bars correspond to the standard deviation among the grain growth rate values composing each data point. Some points lack error bars because fewer than three grains could be measured, due either to a lack of nucleation events (at higher temperature) or to rapid grain impingement (at lower temperature). It was found that $\nu_{spherulite}$ and ν_{major} were equivalent within experimental uncertainty at the measured temperatures. This is reasonable since the major axis is perpendicular to the cylinders in the ellipsoid grains, and the spherulites have cylinders aligned tangentially. That is, both $\nu_{spherulite}$ and ν_{major} are determined by adding cylinders laterally and should therefore have comparable values. The values of ν_{minor} were consistently a factor of 2 smaller than $\nu_{spherulite}$ and ν_{major} at all quench depths. The ratio of ν_{major} to ν_{minor} ranged from 1.8 to 2.3 for the range of temperatures measured, as shown in Figure 9. This is consistent with the observations that the ellipsoid grains consistently had aspect ratios of ca. 2.

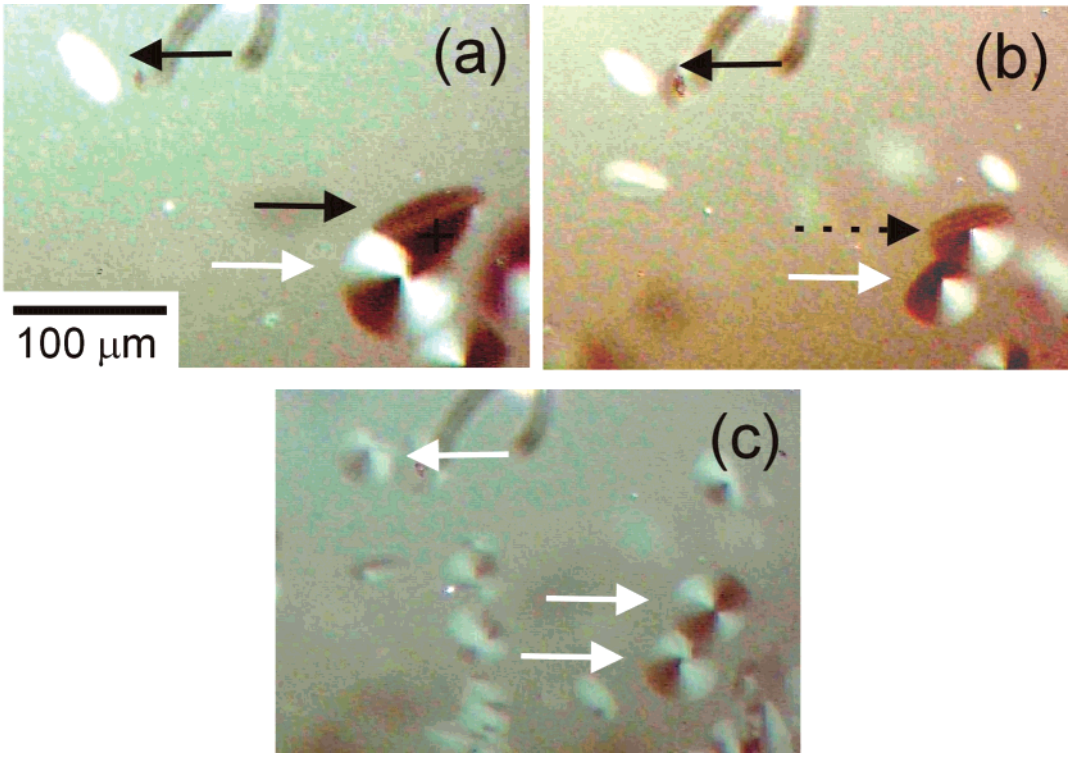

Figure 6. Nucleation at recurring sites for three separate quenches from disorder at a fixed field of view. Three grains that nucleated at identical positions are pointed out. Black arrows point to ellipsoidal grains, white arrows point to spherulites, and dashed arrows point to grains that have partially converted to spherulites. Images were taken (a) 5.0 min after a quench from disorder to 37.5 °C, (b) 3.5 min after a quench from disorder to 37.2 °C, and (c) 2.8 min after a quench from disorder to 36.5 °C.

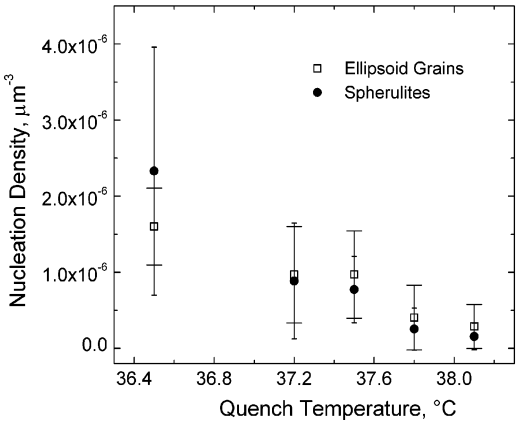

Figure 7. Nucleation density of ellipsoid and spherulite grains for measured quench temperatures.

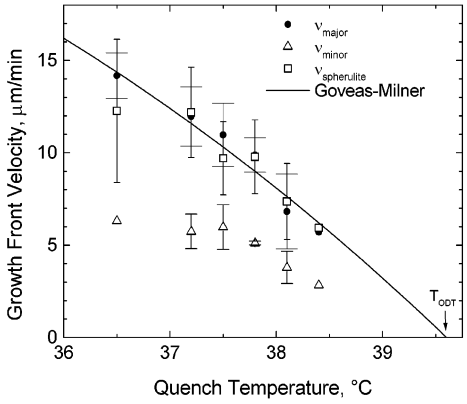

Figure 8. Growth front velocities of individual grains at the measured quench temperatures. Ellipsoid grains are characterized by their major (ν_{major}) and minor (ν_{minor}) axes. The smooth curve corresponds to the scaled prediction of Goveas and Milner (eq 1).

The difference between ν_{major} and ν_{minor} can also help in understanding the presence of spherulites. As was discussed earlier, spherulites grow by adding additional cylinders tangentially. Since this is the most rapid mode of ellipsoid grain growth, it would be unlikely for a spherulite to convert to an ellipsoid, while the reverse is possible. For example, a grain defect or a secondary nucleation event could result in cylinders being mainly aligned tangentially across a nascent grain surface. Because of the different growth rates parallel and perpendicular to the cylinder axis, the formation of new cylinders, expanding laterally, would irrevocably overcome cylinder lengthening, and a spherulite would ultimately result. Thus, the spherulite would be a result of a kinetic "accident" as opposed to a thermodynamic preference. Figure 10 shows an example of a partial transformation. The original ellipoid grain in Figure 10a has a small secondary nucleation event on one site, and by Figure 10d the majority of the grain has a spherulite form with cylinders aligned tangentially to the center of the grain. From observations, it does not appear that this type of event is due to separate grains impinging on one another because it has been observed even in cases where the nucleation density is extremely low.

Balsara and co-workers have recently postulated that prolate ellipsoid grains can be observed when kinetic factors dominate cylinder ordering, and oblate ellipsoids occur when ordering is thermodynamically controlled.[32] They observed prolate ellipsoids for many quenching conditions, $T_{ODT} - T = 3$ °C,[26] $T_{ODT} - T = 3-17$ °C,[21] and $T_{ODT} - T = 4.5-9$ °C,[24] but the presence of oblate ellipsoids has been ruled out only in a deep quench ($T_{ODT} - T = 17$ °C)[32] where kinetic effects are dominant. Oblate ellipsoids have been observed by Sakamoto et

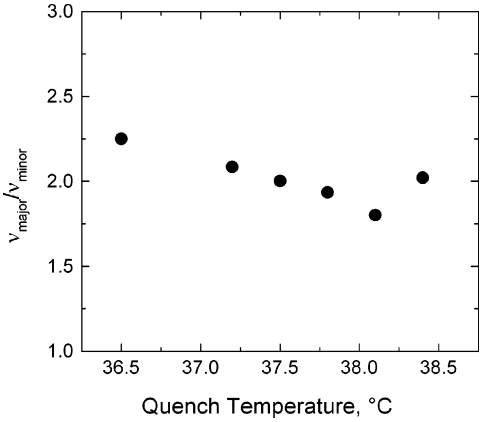

Figure 9. Ratios of ellipsoid major to minor axes growth front velocities for the measured quench temperatures.

al. for a shallow quench ($T_{OOT} - T \approx 5$ °C).[2] Wickham too concluded that oblate ellipsoids would arise, assuming thermodynamic control.[33] Our experiments observe oblate ellipsoids in shallow quenches ($T_{ODT} - T = 1.2-3.1$ °C), a temperature range where thermodynamic factors dominate. From the Goveas−Milner predictions, it is expected that kinetic factors do not begin to dominate until quenches of $T_{ODT} - T > 14.6$ °C. The kinetic effects, however, could contribute at the measured temperatures, given the proximity of kinetically dominated temperatures. That is, the aspect ratio should decrease with increasing quench depth. Figure 9 shows that this was not observed in our system. In fact, the aspect ratio tends to increase slightly at increasing quench depth. Nevertheless, further study of deep quenches is needed to better understand the conditions associated with prolate ellipsoid grain growth.

The experimental growth front velocities were quantitatively compared to a scaleable version of the Goveas and Milner result.[30]

$$v = \frac{\langle h^2 \rangle^{1/2}}{\tau_1}(\chi - \chi_{ODT})g(f)\alpha \qquad (1)$$

where $\langle h^2 \rangle^{1/2}$ is the root-mean-square chain end-to-end distance, τ_1 is the chain relaxation time, $(\chi - \chi_{ODT})$ is the change in Flory−Huggins interaction parameter from T_{ODT} to the measurement temperature, N is the degree of polymerization, $g(f)$ is a constant dependent on block composition, and α is an adjustable scaling parameter that we have incorporated.

Methods for determining the requisite parameters are described elsewhere.[29] The relaxation time of the polymer chain, τ_1, was previously determined from the crossover frequency in $G^*(\omega)$. In this work, however, τ_1 was too small above T_{ODT} for this type of measurement. Instead, τ_1 was estimated from the zero-shear viscosity (η_0) and plateau modulus (G_N) as shown via the reptation relation.

$$\tau_1 = \frac{12}{\pi^2}\frac{\eta_0}{G_N} \qquad (2)$$

The zero-shear viscosity of SI(15−13) in DBP was obtained from the measured frequency dependence of the loss modulus, $G''(\omega)$ above T_{ODT}, as

$$\eta_0 = \lim_{\omega \to 0}\left(\frac{G''}{\omega}\right) \qquad (3)$$

The plateau modulus of the diblock was estimated to be 0.3 MPa from the known plateau moduli of PS and PI homopolymers.[38] The solvent was accounted for by scaling as $G_{N,solution} = G_{N,melt}(0.5)^{2.3}$. At 40.5 °C τ_1 thus estimated was 0.024 s. The temperature dependence of the relaxation time, $\tau_1(T)$, was determined from the Williams−Landel−Ferry equation. The WLF parameters were derived from the data of Jin and Lodge, who characterized a similar sample, SI(16−19) in dioctyl phthalate at the same concentration as the sample measured here.[39]

The smooth curve drawn in Figure 8 represents the scaled Goveas−Milner result. The scaling factor, α, is 3.8. The discrepancy in magnitude may partially arise from uncertainty in the parameters inserted into eq 1. For example, some approximations were made estimating χ, τ_1, and $g(f)$. On the other hand, eq 1 predicts the temperature dependence quite well.

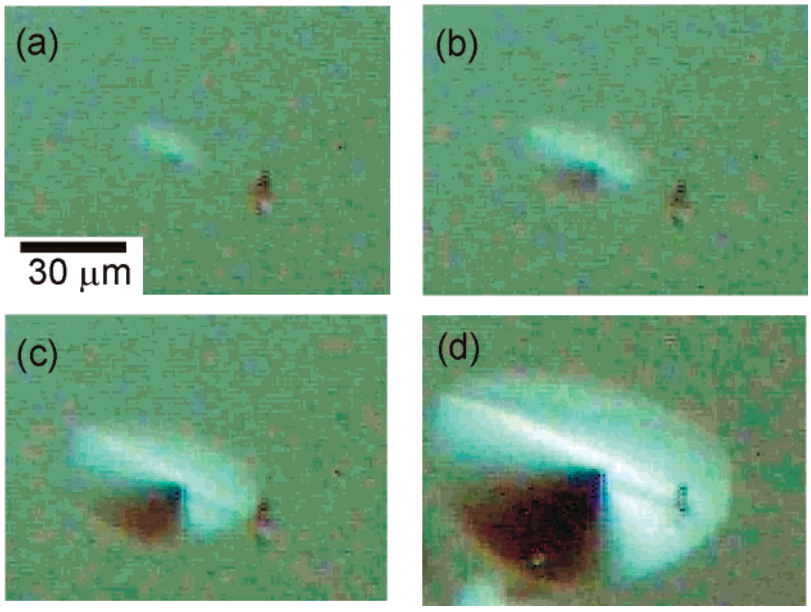

Figure 10. Partial conversion of an ellipsoid grain to a spherulite. Images were taken for a quench from disorder to 37.8 °C after (a) 2.6, (b) 3.3, (c) 4.3, and (d) 6.0 min.

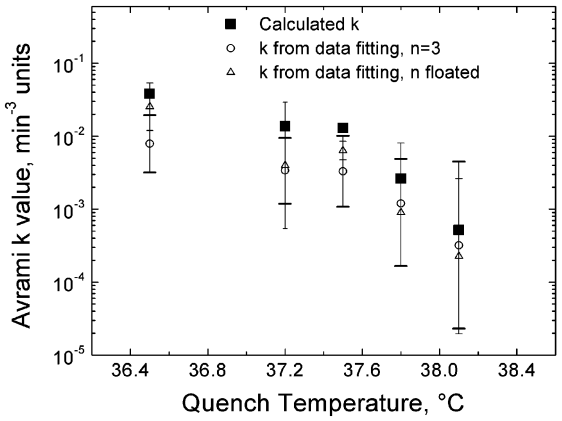

Figure 11. Avrami *k* values calculated from grain growth front velocities and nucleation density along with *k* values obtained from nonlinear curve fitting.

Table 1. Measured Kinetic Parameters and Corresponding Avrami Parameters

T_{quench}, °C	growth rate, μm/min	nucleation density, μm^{-3}	calcd Avrami *k* value, min^{-3}	fitted Avrami *n* exponent
38.1	7.1	3.5×10^{-7}	5.2×10^{-4}	2.8
37.8	9.8	6.6×10^{-7}	2.6×10^{-3}	2.7
37.5	12.1	1.7×10^{-6}	1.3×10^{-2}	2.6
37.2	12.1	1.9×10^{-6}	1.4×10^{-2}	2.8
36.5	13.2	3.9×10^{-6}	3.8×10^{-2}	2.8

Analysis of Bulk Kinetics. The "bulk" kinetics could be characterized by measuring the area fraction of the cylinder phase formed across the entire field of view. This was done by visually identifying birefringent regions and manually tracing them. In this way the ordered cylinder fraction, ϕ_c, was determined as a function of time for each quench experiment. Typically this type of data is fit to the Avrami equation (eq 4) to gain insight into the nucleation and growth mechanism.

$$\phi_c = 1 - \exp(-kt^n) \tag{4}$$

The Avrami equation has parameters *k* and *n*. The value of *n* depends on whether heterogeneous or homogeneous nucleation is dominant and the grain shape. Direct observation of the POM micrographs shows that heterogeneous nucleation was most common. Heterogeneous nucleation was observed in several ways, including direct observation of heterogeneous nucleating agents, as was discussed above. Furthermore, three-dimensional growth occurred, which means that an *n* value of 3 is expected. The rate constant, *k*, depends on the nucleation density and growth front velocity; in this case $k = {}^4/_3\pi\nu^3 L$, where ν is the grain growth front velocity and *L* is the nucleation density. The calculated *k* values using experimental values of ν and *L* are listed in Table 1. Values for *k* can also be obtained independently by fitting the time dependence of ϕ_c to the Avrami equation. Nonlinear curve fitting of the Avrami equation was performed both with *n* fixed at 3 and with *n* not fixed. The results are shown in Figure 11. There is good agreement among the different *k* values for all quench temperatures. Note that the "fitted" values were obtained by fitting individual quench experiments and averaging the resulting *k* values. There is considerable variation in the data at any given quench temperature, as evidenced by the error bars. The major reason for this is the limited field of view.

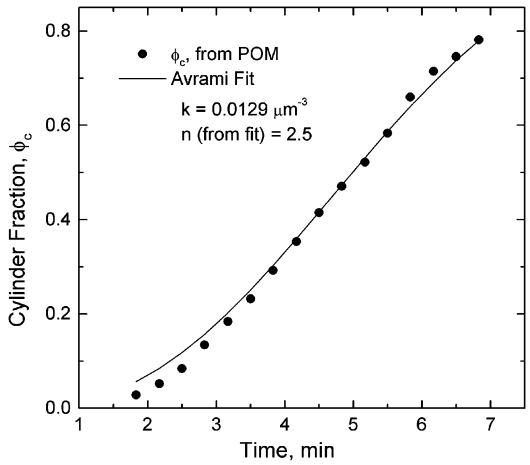

Figure 12. Fraction of cylinder, ϕ_c, measured from POM for a quench to 37.5 °C. The data are fit to the Avrami equation using the *k* value calculated from the observed growth front velocity and nucleation density. The *n* value is extracted from the fit.

Estimates of *n* were made by fitting $\phi_c(t)$ while fixing *k* at the values shown in Table 1. Figure 12 shows a typical Avrami fit to the POM data. Fits were made to each quench experiment, and the averaged *n* values for each temperature are listed in Table 1. For all quench temperatures, the average *n* values were slightly below the expected value of 3. This is in good agreement with the results of Floudas et al.[8] The *n* value may be lower than expected because of the anisotropy of the grains, where the presence of the slow growth axis could lead to a slightly lower *n*. In addition, there are limitations to using microscopy to describe bulk kinetics. As described above, the ensemble average value had to be approached by averaging separate quench measurements due to the limited field of view. Also, at the lower quench temperatures, the large amounts of small grains caused superposition of grains, leading to uncertainty in determining ϕ_c. Considering the simplicity of the Avrami model and the aforementioned uncertainties, the agreement should be considered good.

Summary

The ordering kinetics of the cylinder phase were measured for poly(styrene-*b*-isoprene) in dibutyl phthalate. Temperature quenches through T_{ODT} were measured with polarizing optical microscopy (POM). The ordering was observed to occur by heterogeneous nucleation followed by three-dimensional growth. The grains had either spherulite or oblate-ellipsoid shape, with roughly equal proportions of both at all quench temperatures. The oblate-ellipsoid grains had an aspect ratio of 2, and cylinders aligned parallel to the minor ellipsoid axis. Detailed characterization of the three-dimensional shape of individual grains showed the oblate ellipsoid to be of "clamlike" shape. The spherulites had cylinders aligned mainly tangentially. Growth front velocities of individual grains were measured and found to be constant throughout the ordering process. The spherulite grains grew at the same rate as the major axis of the ellipsoid grains. These both grew at 2 times the rate of the minor axis. The predictions of the Goveas−Milner expression were quantitatively compared to measured grain growth front velocities, and good agreement was observed for the temperature dependence. Avrami analysis matched well with the

directly observed nucleation and growth mechanism. Thus, POM was an effective tool in characterizing grain shape, individual grain growth front velocities, and bulk kinetics.

Acknowledgment. This work was supported by the National Science Foundation through Award DMR-9901087.

References and Notes

(1) Sakamoto, N.; Hashimoto, T. *Macromolecules* **1998**, *31*, 3292.
(2) Sakamoto, N.; Hashimoto, T. *Macromolecules* **1998**, *31*, 8493.
(3) Hashimoto, T.; Sakamoto, N. *Macromolecules* **1995**, *28*, 4779.
(4) Kim, J. K.; Lee, H. H.; Ree, M.; Lee, K.-B.; Park, Y. *Macromol. Chem. Phys.* **1998**, *199*, 641.
(5) Hashimoto, T.; Ogawa, T.; Sakamoto, N.; Ichimiya, M.; Kim, J. K.; Han, C. D. *Polymer* **1998**, *39*, 1573.
(6) Adams, J. L.; Quiram, D. J.; Graessley, W. W.; Register, R. A.; Marchand, G. R. *Macromolecules* **1996**, *29*, 2929.
(7) Floudas, G.; Pakula, T.; Fischer, E. W.; Hadjichristidis, N.; Pispas, S. *Acta Polym.* **1994**, *45*, 176.
(8) Floudas, G.; Hadjichristidis, N.; Iatrou, H.; Pakula, T.; Fischer, E. W. *Macromolecules* **1994**, *27*, 7735.
(9) Migler, K. B.; Han, C. C. *Macromolecules* **1998**, *31*, 360.
(10) Hajduk, D. A.; Tepe, T.; Takenouchi, H.; Tirrell, M.; Bates, F. S.; Almdal, K.; Mortensen, K. *J. Chem. Phys.* **1998**, *108*, 326.
(11) Gupta, J. A.; Singh, M. A.; Salomons, G. J.; Foran, W. A.; Capel, M. S. *Macromolecules* **1998**, *31*, 3109.
(12) Takenaka, M.; Linliu, K.; Ying, Q.; Chu, B.; Peiffer, D. *Macromolecules* **1995**, *28*, 2700.
(13) Stuehn, B.; Vilesov, A.; Zachmann, H. G. *Macromolecules* **1994**, *27*, 3560.
(14) Shannon, R. F., Jr.; Glavicic, M. G.; Singh, M. A. *J. Macromol. Sci., Phys.* **1994**, *B33*, 357.
(15) Singh, M. A.; Harkless, C. R.; Nagler, S. E.; Shannon, R. F.; Ghosh, S. S. *Phys. Rev. B: Condens. Matter* **1993**, *47*, 8425.
(16) Schuler, M.; Stuehn, B. *Macromolecules* **1993**, *26*, 112.
(17) Harkless, C. R.; Singh, M. A.; Nagler, S. E.; Stephenson, G. B.; Jordan-Sweet, J. L. *Phys. Rev. Lett.* **1990**, *64*, 2285.
(18) Rosedale, J. H.; Bates, F. S. *Macromolecules* **1990**, *23*, 2329.
(19) Bates, F. S.; Rosedale, J. H.; Fredrickson, G. H. *J. Chem. Phys.* **1990**, *92*, 6255.
(20) Kim, W. G.; Chang, M. Y.; Garetz, B. A.; Newstein, M. C.; Balsara, N. P.; Lee, J. H.; Hahn, H.; Patel, S. S. *J. Chem. Phys.* **2001**, *114*, 10196.
(21) Kim, W. G.; Garetz, B. A.; Newstein, M. C.; Balsara, N. P. *J. Polym. Sci., Part B: Polym. Phys.* **2001**, *39*, 2231.
(22) Newstein, M. C.; Garetz, B. A.; Balsara, N. P.; Chang, M. Y.; Dai, H. J. *Macromolecules* **1998**, *31*, 64.
(23) Balsara, N. P.; Garetz, B. A.; Newstein, M. C.; Bauer, B. J.; Prosa, T. J. *Macromolecules* **1998**, *31*, 7668.
(24) Balsara, N. P.; Garetz, B. A.; Chang, M. Y.; Dai, H. J.; Newstein, M. C.; Goveas, J. L.; Krishnamoorti, R.; Rai, S. *Macromolecules* **1998**, *31*, 5309.
(25) Pan, L. H.; Singh, M. A.; Salomons, G. J.; Gupta, J. A.; Capel, M. S. *J. Macromol. Sci., Phys.* **1996**, *B35*, 749.
(26) Dai, H. J.; Balsara, N. P.; Garetz, B. A.; Newstein, M. C. *Phys. Rev. Lett.* **1996**, *77*, 3677.
(27) Floudas, G.; Fytas, G.; Hadjichristidis, N.; Pitsikalis, M. *Macromolecules* **1995**, *28*, 2359.
(28) Sakamoto, N.; Hashimoto, T. *Macromolecules* **1998**, *31*, 3815.
(29) Chastek, T. Q.; Lodge, T. P. *Macromolecules* **2003**, *36*, 7672.
(30) Goveas, J. L.; Milner, S. T. *Macromolecules* **1997**, *30*, 2605.
(31) Koizumi, S.; Hasegawa, H.; Hashimoto, T. *Macromolecules* **1994**, *27*, 6532.
(32) Abuzaina, F. M.; Garetz, B. A.; Mody, J. U.; Newstein, M. C.; Balsara, N. P. *Macromolecules* **2004**, *37*, 4185.
(33) Wickham, R. A.; Shi, A.-C.; Wang, Z.-G. *J. Chem. Phys.* **2003**, *118*, 10293.
(34) Lodge, T. P.; Pudil, B.; Hanley, K. J. *Macromolecules* **2002**, *35*, 4707.
(35) Hashimoto, T.; Sakamoto, N.; Koga, T. *Phys. Rev. E* **1996**, *54*, 5832.
(36) Chang, M. Y.; Abuzaina, F. M.; Kim, W. G.; Gupton, J. P.; Garetz, B. A.; Newstein, M. C.; Balsara, N. P.; Yang, L.; Gido, S. P.; Cohen, R. E.; Boontongkong, Y.; Bellare, A. *Macromolecules* **2002**, *35*, 4437.
(37) Balsara, N. P.; Marques, C. M.; Garetz, B. A.; Newstein, M. C.; Gido, S. P. *Phys. Rev. E* **2002**, *66*, 052802/1.
(38) Fetters, L. J.; Lohse, D. J.; Richter, D.; Witten, T. A.; Zirkel, A. *Macromolecules* **1994**, *27*, 4639.
(39) Jin, X.; Lodge, T. P. *Rheol. Acta* **1997**, *36*, 229.

MA049502D